Fluorescent, Superparamagnetic Nanospheres for Drug Storage, Targeting, and Imaging: A Multifunctional Nanocarrier System for Cancer Diagnosis and Treatment

Hoon-Sung Cho,[†] Zhongyun Dong,[‡] Giovanni M. Pauletti,[§] Jiaming Zhang,[⊥] Hong Xu,[∥] Hongchen Gu,[∥] Lumin Wang,[⊥] Rodney C. Ewing,[⊥] Christopher Huth,[†] Feng Wang,[†] and Donglu Shi[#,†,*]

[†]School of Energy, Environmental, Biological and Medical Engineering, University of Cincinnati, Cincinnati, Ohio 45221, [‡]Department of Internal Medicine, College of Medicine, University of Cincinnati, Cincinnati, Ohio 45221, [§]James L. Winkle College of Pharmacy, University of Cincinnati, Cincinnati, Ohio 45267, [⊥]Departments of Geological Sciences, Nuclear Engineering & Radiological Sciences and Materials Science & Engineering, University of Michigan, Ann Arbor, Michigan 48109, [∥]Med-X Institute, Shanghai Jiao Tong University, Shanghai 200030, China, and [#]The Institute for Advanced Materials and Nano Biomedicine, Tongji University, Shanghai, China 200092

ABSTRACT For early cancer diagnosis and treatment, a nanocarrier system is designed and developed with key components uniquely structured at nanoscale according to medical requirements. For imaging, quantum dots with emissions in the near-infrared range (~800 nm) are conjugated onto the surface of a nanocomposite consisting of a spherical polystyrene matrix (~150 nm) and the internally embedded, high fraction of superparamagnetic Fe_3O_4 nanoparticles (~10 nm). For drug storage, the chemotherapeutic agent paclitaxel (PTX) is loaded onto the surfaces of these composite multifunctional nanocarriers by using a layer of biodegradable poly(lactic-*co*-glycolic acid) (PLGA). A cell-based cytotoxicity assay is employed to verify successful loading of pharmacologically active drug. Cell viability of human, metastatic PC3mm2 prostate cancer cells is assessed in the presence and absence of various multifunctional nanocarrier populations using the MTT assay. PTX-loaded composite nanocarriers are synthesized by conjugating anti-prostate specific membrane antigen (anti-PSMA) for targeting. Specific detection studies of anti-PSMA-conjugated nanocarrier binding activity in LNCaP prostate cancer cells are carried out. LNCaP cells are targeted successfully *in vitro* by the conjugation of anti-PSMA on the nanocarrier surfaces. To further explore targeting, the nanocarriers conjugated with anti-PSMA are intravenously injected into tumor-bearing nude mice. Substantial differences in fluorescent signals are observed *ex vivo* between tumor regions treated with the targeted nanocarrier system and the nontargeted nanocarrier system, indicating considerable targeting effects due to anti-PSMA functionalization of the nanocarriers.

KEYWORDS: quantum dot · targeting · fluorescent imaging · drug storage · magnetic nanosphere

One of the critical challenges in early cancer diagnosis and treatment by nanotechnology is the development of multifunctional particles at the nanoscale that simultaneously serve as sensitive, cell-specific bioprobes and localized tumor treatment. Extensive efforts have been devoted to designing nanocarriers that combine cell targeting with efficient *in vivo* imaging, drug storage, and controlled drug release capabilities.[1−3] Specific material features required to implement these properties include surface functional groups suitable for bioconjugation and fluorescent imaging modules in addition to controlled drug storage and release mechanisms. On the basis of specific medical requirements, the multifunctional nanocarriers must also be biocompatible. For effective early cancer diagnosis and treatment, the colloidal nanocarriers are required to be less than 200 nm in diameter[4,5] and monodispersed to achieve efficient distributions in the targeted tumor lesions. Spherical shape is preferred as it facilitates uniform surface conjugation of cell-targeting ligands (*e.g.*, antibodies) and imaging probes. Fluorescent emission near 800 nm is most suitable for deep tissue *in vivo* imaging.[6] Incorporation of superparamagnetic properties into nanocarriers further benefits medical applications by facilitating multimodal imaging, hyperthermia therapy, and magnetic manipulation.[7−9]

Previously, we reported on the design of unique, fluorescent, magnetic nanospheres (MNSs) that allow effective *in vivo* imaging due to their strong fluorescence emissions of surface-conjugated quantum dots (QDs). Our experimental results indicated that these MNSs successfully induced hyperthermia under an alternating magnetic field.[10] The fabricated MNSs had an average diameter around 150 nm and were composed of Fe_3O_4 nanoparticles

*Address correspondence to shid@ucmail.uc.edu.

Received for review May 7, 2010 and accepted August 05, 2010.

Published online Xxxxxxxxx 00, 0000
10.1021/nn101000e

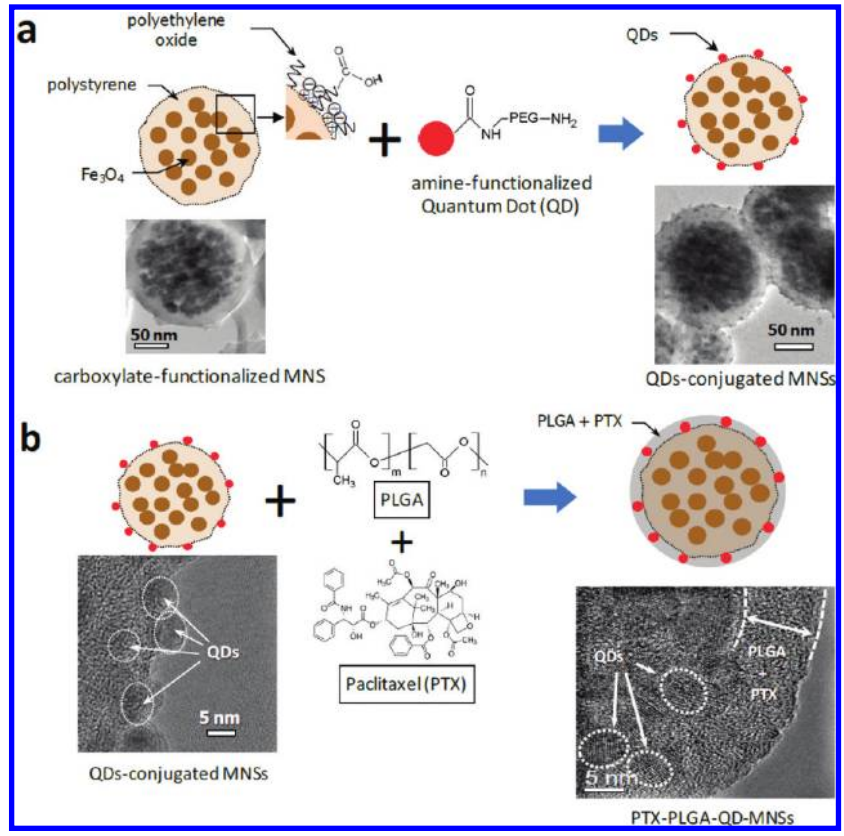

Figure 1. Schematic diagrams illustrating surface functionalization of MNSs: (a) conjugation of amine-functionalized quantum dots (QDs) to the surface of carboxylate-functionalized MNSs using conventional NHS/EDC coupling method; (b) PTX loading using a thin PLGA coat on the surface of QD-MNSs.

(~15−20 nm in diameter) embedded in a polystyrene matrix. TGA analysis shows that the weight ratio of the embedded Fe_3O_4 nanoparticles to polystyrene in MNS is 4:1.[11] QDs were covalently conjugated to the surface of these MNSs using standard carbodiimide chemistry. Our results demonstrated strong *in vivo* and *ex vivo* fluorescence that facilitated biodistribution monitoring of multifunctional, fluorescent MNSs in mice. In addition, the high volume fraction of magnetite was sufficient to induce hyperthermia that can be utilized for tumor cell suppression and drug release control.

In this study, we have further advanced the multifunctional nanosystem by tailoring the surfaces of MNSs with therapeutic modality including cell targeting and drug storage capabilities. In this way, the multifunctional nanosystem will be fully developed specifically for preclinical applications including *in vivo* imaging, cell targeting, and drug storage. Note that these functionalities can be potentially utilized simultaneously within one nanosystem for cancer diagnosis and chemotherapy.[12,13]

RESULTS AND DISCUSSION

Figure 1 depicts the unique composite structure with nanosized Fe_3O_4 particles embedded inside a spherical polystyrene matrix. The QDs are conjugated onto the MNSs for effective *in vivo* imaging. Combining QDs and Fe_3O_4 nanoparticles in the same MNS enables two-mode imaging by fluorescence and magnetic resonance, respectively. This would effectively enhance the imaging capabilities for clinical versatility. Furthermore, the new design allows concurrent pharmacological intervention at the tumor site mediated by the chemotherapeutic agent paclitaxel (PTX) that is loaded onto the surface of these MNSs using a layer of biodegradable poly(lactic-*co*-glycolic acid) (PLGA). PTX is a microtubule-stabilizing agent that is clinically administered to treat various solid tumors.[14−17] PLGA is a biocompatible and FDA-approved copolymer that allows diffusion- and erosion-controlled drug release and, in addition, is sensitive to temperature-dependent degradation.[18−20] Both PTX and PLGA have been extensively used in current drug delivery research focused on cancer therapies.[21−24]

The schematic diagram in Figure 1 illustrates the basic components of the multifunctional nanocarrier design. Covalent conjugation of amine-functionalized, fluorescent QDs to the surface of carboxylate-functionalized, polyethylene oxide modified MNSs is achieved using the conventional EDC/NHS coupling method. Microscopically, the surface modification can be visualized in Figure 1a by a change in the smooth surface structure of the original MNS (transmission electron microscopy image on the left) to a dark spotted, ruffled surface (transmission electron microscopy image on the right) after QD conjugation. Surface-

immobilized QDs are more clearly identified by their distinctive lattice structures seen in the high-resolution transmission electron micrographs (HRTEM, Figure 1b). Previous research from our laboratory employed similar coupling strategies to conjugate near-infrared QDs to polystyrene-Fe_3O_4 composite nanospheres for *in vivo* fluorescent imaging.[10]

In this study, QDs with a visible emission wavelength of 655 nm were selected for the *in vitro* cell imaging experiments, and QDs with a near-infrared emission wavelength of 800 nm were used for the *in vivo* and *ex vivo* imaging. After conjugation of QDs to MNSs, PTX was incorporated into the fluorescent nanocarrier using a drug-loaded PLGA coating layer (PTX-PLGA-QD-MNSs). The transmission electron micrograph (TEM) in Figure 1b clearly shows a uniform, 7−10 mm thick PLGA layer surrounding the QD-MNS surface boundary. As PTX cannot be distinguished microscopically from the PLGA matrix, a cell-based cytotoxicity assay was employed to verify successful loading of a pharmacologically active drug.

Cell viability of human, metastatic PC3mm2 prostate cancer cells was assessed in the presence and absence of various MNS populations using the MTT assay. Figure 2 shows that incubation of these tumor cells with a broad dosing range of unmodified MNS, QD-labeled, fluorescent MNSs, and PLGA-coated, fluorescent MNSs does not significantly affect mitochondrial dehydrogenase activity as compared to vehicle control. These results experimentally underline the safety of drug-free, fluorescent nanocarriers up to 25 μg/mL. In contrast, PTX-PLGA-QD-MNSs dose-dependently decreased cell viability of human PC3mm2 prostate cancer cells *in vitro* after a 96 h incubation. The estimated PTX-PLGA-QD-MNS concentration associated with 50% inhibition of the mitochondrial enzyme activity (IC_{50}) was 125 ng/mL. Previously, we determined that the IC_{50} value of solubilized paclitaxel in the same cancer cell line is 5 ng/mL.[25] As cytotoxic efficacy of PTX-PLGA-QD-MNS is associated with solubilized PTX, we estimate that approximately 0.5 ng of PTX was released from the PLGA drug storage compartment leading to a free PTX concentration of 5 ng/mL. Therapeutically, the relationship between drug loading capacity of colloidal nanocarriers and drug release rate is of utmost importance. Consequently, further experiments are planned to quantify drug loading efficiency and time-dependent release properties from these multifunctional MNSs using different fabrication procedures, including double emulsion and organic coating methods.

To confirm the role of PLGA copolymer as a drug-holding and drug-releasing substance, the loading efficacy of paclitaxel on the MNSs according to the different ratio of PLGA was estimated *in vitro* by the MTT assay. For this purpose, the amount of PLGA was doubled or reduced by half from the original volume. It is shown that the cell viabilities are decreased by increasing the amount of PLGA used for paclitaxel loading (Figure 3). This indicates that the increased volume

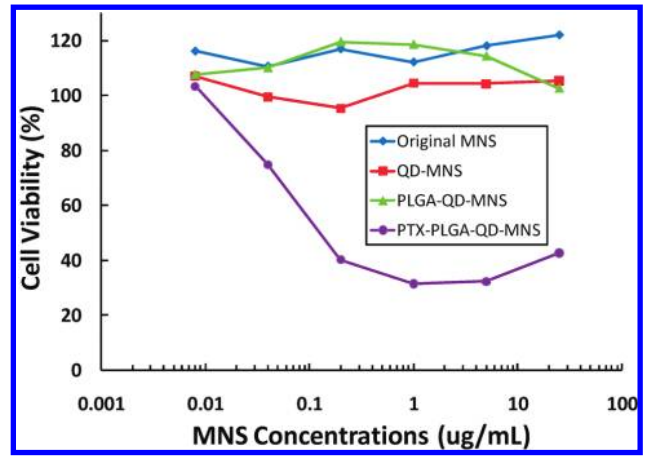

Figure 2. Dose-dependent effects of MNSs, QD-MNS, PLGA-QD-MNS, and PTX-PLGA-QD-MNSs on viability of human PC3mm2 prostate cancer cells. Tumor cells were treated for 96 h with various doses of drug-free or PTX-containing MNSs dispersed in EMEM/5% FBS. Cell viability was assessed using the MTT assay.

of PLGA on the surface of MNSs may have enhanced paclitaxel loading efficiency on the MNSs. However, it is observed that the variations of cell viabilities according to decreasing dosages of paclitaxel-loaded MNSs show the same increasing rates regardless of the ratio of paclitaxel to PLGA, which means that *in vitro* drug release behavior is not affected by the volume of PLGA, coated on the MNSs. It has been reported that the *in vitro* drug release from the paclitaxel-loaded PLGA nanoparticles exhibit less than 30% of encapsulated drug after 10 days.[26] This suggests that the characteristics of PLGA copolymer, such as the variation of monomer ratio by breaking the ester linkages, or the glass transition temperature, may have been changed during the process of a sequences of dissolving in dichloromethane (DCM) and reprecipitating in an aqueous solution, phosphate buffered saline (PBS).

Recently, it was reported that particle-associated PTX accumulates more efficiently than solubilized drug in tumor models *in vivo*.[27] Since intracellular PTX concentration directly correlates with tumor cell kill, the cellular binding and transport studies were carried out in

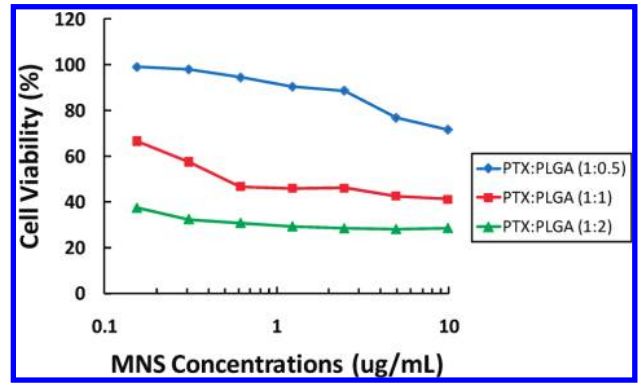

Figure 3. Drug loading effects on the MNSs according to the ratio of paclitaxel (PTX) and PLGA by viability of human PC3mm2 prostate cancer cells. Tumor cells were treated for 4 days with various amounts of MNSs or drug-loaded MNSs dispersed in culture media supplemented with 5% fetal bovine serum for 4 days.

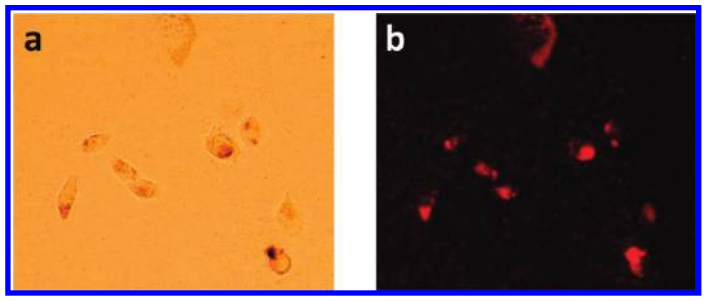

Figure 4. Cellular interaction of PTX-PLGA-QD-MNSs with human PC3mm2 prostate cancer cells evaluated by fluorescence microscopy: (a) optical image of live PC3mm2 cells incubated with PTX-PLGA-QD-MNSs, and (b) fluorescence image of PC3mm2 cells incubated with PTX-PLGA-QD-MNS (EX = 560/40 nm, EM = 620/40 nm).

this research to understand the mechanisms by which polymeric PTX particles are taken up into cells. The results showed a significant contribution of caveolin-dependent, receptor-mediated endocytosis of intact particles augmenting intracellular PTX concentrations. To determine whether similar endocytic pathways exist in human PC3mm2 prostate cancer cells, cellular uptake of PTX-PLGA-QD-MNSs was assessed by fluorescence microscopy. The optical image in Figure 4a clearly shows the cellular boundaries of PC3mm2 cancer cells. The same field visualized under fluorescence (EX = 560/40 nm, EM = 620/40 nm) demonstrates strong emission of MNS-immobilized QDs that appear to reside in the cytosol (Figure 4b). Without *z*-stack images acquired by confocal laser scanning microscopy, it cannot be verified whether PTX-PLGA-QD-MNSs successfully accumulated inside the cancer cells. However, even close association of drug-loaded, fluorescent MNSs with the cell membrane is predicted to enhance the therapeutic index of PTX as a consequence of improved tumor targeting. Further studies are required to delineate molecular events underlying increased binding to and/or uptake of PTX-PLGA-QD-MNSs into human PC3mm2 prostate cancer cells.

Targeted PTX-PLGA-QD-MNSs were synthesized by conjugating anti-prostate specific membrane antigen (anti-PSMA) on the PTX-PLGA-QD-MNSs for *in vitro* and *in vivo* targeting (Figure 5). The surface of QD-MNSs was carboxyl-functionalized using carboxyl-terminated PLGA with incorporation of PTX. The anti-PSMA was

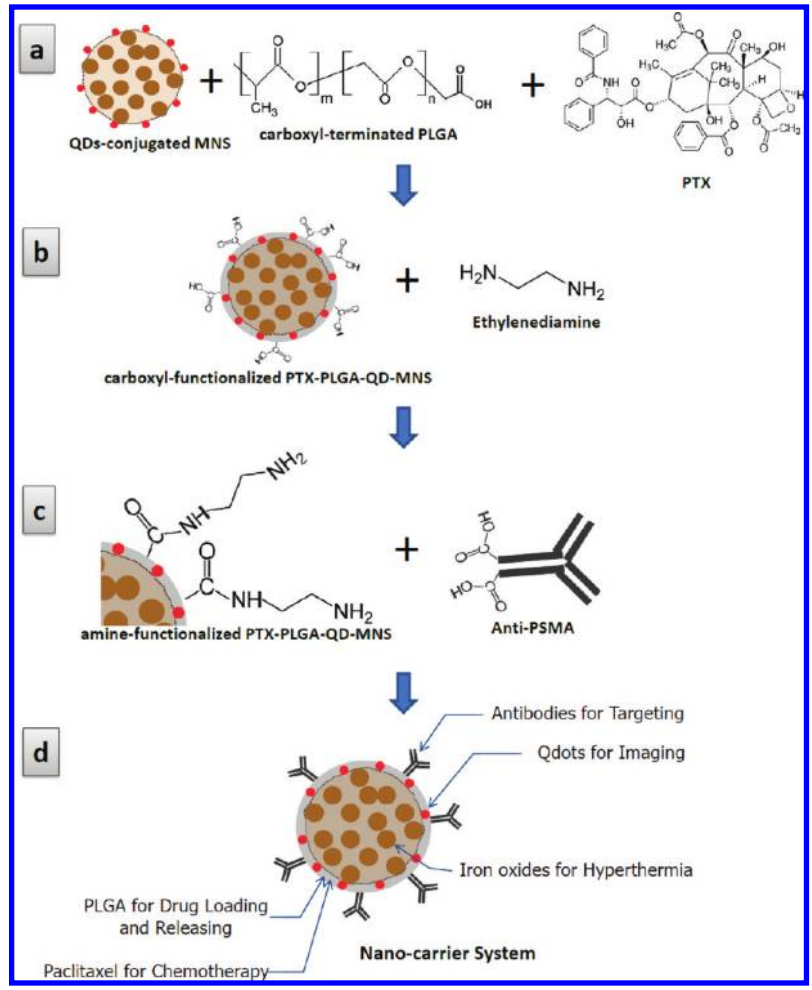

Figure 5. Schematic diagrams illustrating surface functionalization of MNSs: (a) carboxyl functionalization using carboxyl-terminated PLGA on the surface of QD-MNSs with PTX loading; (b) amine functionalization by conjugation of ethylenediamine to the surface of carboxylate-functionalized PTX-PLGA-QD-MNSs using conventional NHS/EDC coupling method; (c) conjugation of anti-PSMA to the PTX-PLGA-QD-MNSs, and (d) new multifunctional (fluorescent imaging, targeting, hyperthermia, and chemotherapy) nanocarrier system.

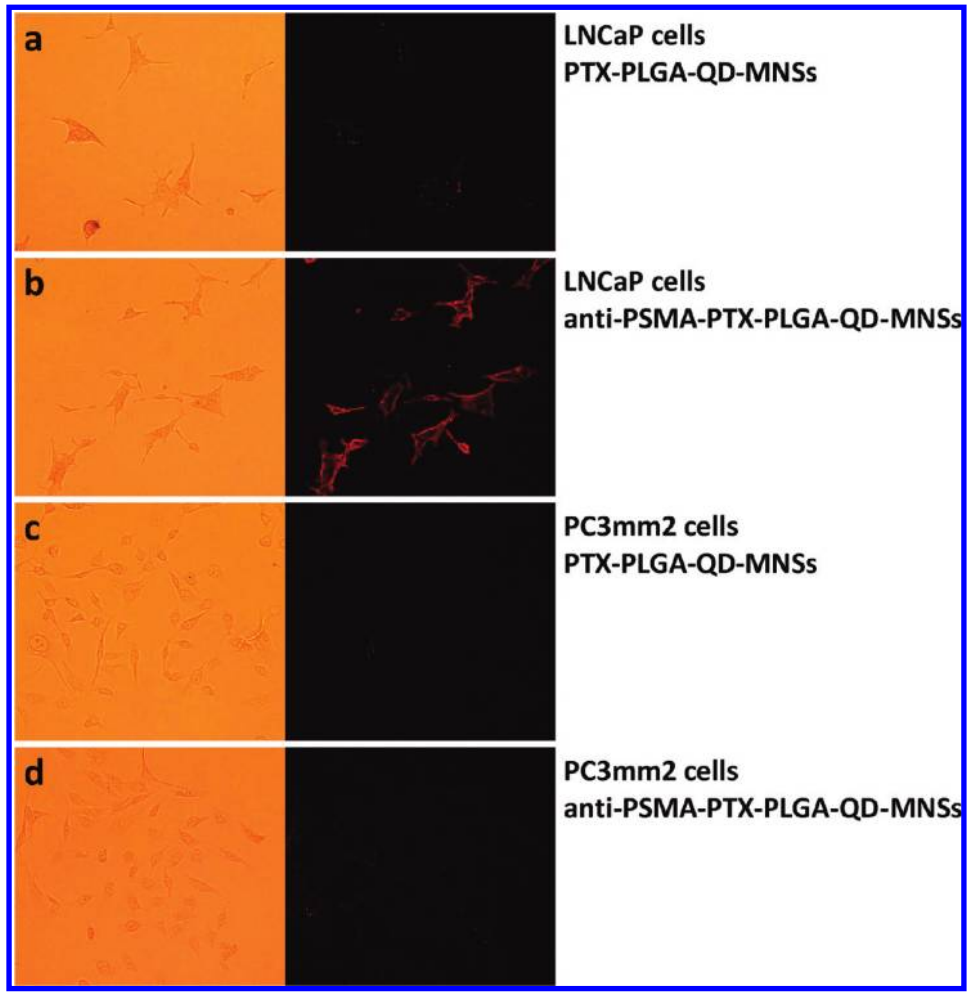

Figure 6. ***In vitro*** **targeting studies of anti-PSMA-conjugated PTX-PLGA-QD-MNSs' binding activity in cultured LNCaP prostate cancer cells, which are PSMA-positive, and PC3mm2, which are known as PSMA-negative.**

coupled to PTX-PLGA-QD-MNSs through ethylenediamine using the conventional EDC/NHS coupling method. In this fashion, the novel multifunctional nanocarrier system (anti-PSMA-PTX-PLGA-QD-MNSs) was composed with multiple components: targeted antibodies, fluorescent probes, chemotherapeutic agents, and superparamagnetic nanoparticles, ideally suited for early cancer diagnosis and treatment.

For cancer cell targeting, specific detection studies have been carried out on the anti-PSMA-conjugated MNSs' binding activity in LNCaP prostate cancer cells. Anti-PSMA-PTX-PLGA-QD-MNSs and nontargeted PTX-PLGA-QD-MNS, as a control, were incubated with the fixed LNCaP and PC3mm2 prostate cancer cells, respectively (Figure 6). Substantially different behaviors are observed between the targeted PTX-PLGA-QD-MNSs and the nontargeted PTX-PLGA-QD-MNSs. LNCaP cells, which express PSMA, are targeted successfully by the conjugation of anti-PSMA on the PTX-PLGA-QD-MNSs surface (Figure 6b). No fluorescent signals were detected in LNCaP cells exposed to nontargeted PTX-PLGA-QD-MNS (Figure 6a). In contrast, PC3mm2 human prostate cells, which are known as PSMA-negative, show no fluorescent signals with and without anti-PSMA conjugation (Figure 6c,d). The binding activity of anti-PSMA to LNCaP cancer cells was also confirmed by immunocytochemical studies using Alexa Fluor 594 F(ab')2 fragment of goat anti-mouse IgG (H+L) as a secondary antibody (data not shown). These results indicate that the specific targeting to cancer cells can be effectively achieved by the multifunctional nanocarrier system.

To further explore the effects of targeting, the biodistribution of the nanocarriers administrated *via* tail vein was analyzed. The PTX-PLGA-QD-MNSs conjugated with anti-PSMA were intravenously injected into a tumor-bearing nude mouse. This study was approved by the Institutional Animal Use and Care Committee (IACUC) at the University of Cincinnati in compliance with relevant State and Federal Regulations. Thirty minutes after injection of the nanocarrier system, the PTX-PLGA-QD-MNSs were biodistributed in various organs of the mouse. These organs were then harvested and compared with a nontreated mouse as a control. *Ex vivo* images were initially taken under the condition for the original emission wavelength of the quantum dot (excitation wavelength = 720 nm, emission wavelength = 790 nm). As shown in Figure 7, *ex vivo* fluorescence im-

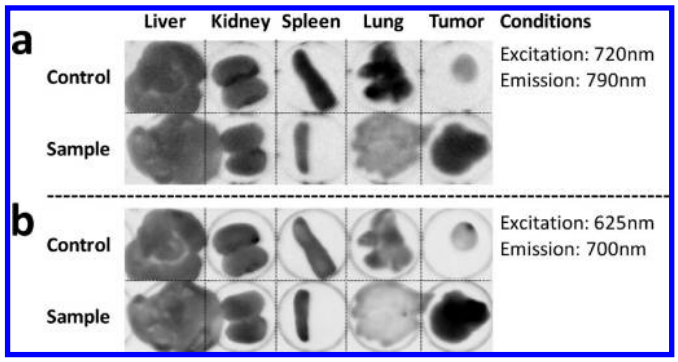

Figure 7. Fluorescent images of excised organs in mice. The images of organs and tumor from the sample mouse injected with anti-PSMA-PTX-PLGA-QD-MNSs are compared with those of the nontreated control mouse.

ages of the tumor indicate an accumulation of the nanocarrier system in this organ of the treated mouse. No significant fluorescence in the tumor was measured in the untreated control animal. As can be seen in Figure 7a, there is a considerable fluorescent signal in the tumor region. It was found that the fluorescent signal was significantly enhanced by using a lower wavelength filter set (excitation wavelength = 625 nm, emission wavelength = 700 nm). Under this condition, the tumor shows sharper contrast of fluorescent signals associated with the nanocarrier system compared to the original condition (Figure 7b). This is due to the emission peak of quantum dot being blue-shifted during sample preparation. This difference is a strong indication that the fluorescent signals from the tumor region are associated with the nanocarriers accumulated as a result of targeting. The current research deals with a systematic *in vivo* targeting imaging study on tumor-bearing mice with intravenously injected anti-PSMA-PTX-PLGA-QD-MNSs.

CONCLUSIONS

We have developed a multifunctional nanocarrier system for medical diagnosis and treatment. This unique system is composed of several key components, namely, fluorescent superparamagnetic nanoparticles for multimodal imaging and hyperthermia, tumor-specific antibodies for cell targeting, and anticancer drugs for localized treatment. The unique nanostructures and surfaces are designed and developed according to biomedical requirements and procedures so that these functionalities may be effectively utilized clinically, allowing simultaneous cancer diagnosis and therapy. Experimental evidence from *in vitro* studies suggests acceptable safety profiles for drug-free, fluorescent PLGA-QD-MNSs. However, inclusion of PTX inside a biocompatible PLGA copolymer layer transforms this multifunctional nanocarrier into an effective therapeutic strategy. In addition to the chemotherapeutic treatment, the nanocarrier system is able to target specific cancer cells and *ex vivo* organs. Further clinical development of the PTX-PLGA-QD-MNS concept as a novel, targeted imaging and drug delivery system may benefit cancer patients in the future due to significantly reduced systemic toxicity and greatly improved noninvasive monitoring capabilities.

METHODS

Surface Conjugation of QDs to MNSs: Carboxylate-functionalized MNSs were washed three times with phosphate-buffered saline, pH 7.4 (PBS), and incubated for 20 min at room temperature in 1-(3-dimethylaminopropyl)-3-ethylcarbodiimide hydrochloride (EDC) solution (100 μL of 400 mM in PBS) and *N*-hydroxysuccinimide (NHS) solution (100 μL of 100 mM in PBS). Excess coupling reagent was removed by magnetic separation. The NHS-activated MNSs were conjugated to amino-functionalized QDs [Qdot 655 ITK amino (PEG), Invitrogen Corp., Carlsbad, CA] following procedures previously published by this laboratory.[5,18] QD-MNSs were washed three times with PBS and stored in 200 μL of PBS until used.

PTX Loading of QD-MNSs: A suspension of 1 mg of QD-MNSs, 100 μg of PTX, and 100 μg of PLGA in 100 μL of acetonitrile was mixed using a sonication bath. Drug-free nanocarriers were fabricated as controls. The organic suspension was added to 500 mL of Milli-Q purified water and emulsified by sonication using an energy output of 5 W. The organic solvent was removed from the oil-in-water emulsion under reduced pressure. PTX-PLGA-QD-MNSs and drug-free control carriers were washed three times in PBS and stored at 4 °C until used.

Synthesis of Amine-Functionalized PTX-PLGA-QD-MNSs: A suspension of 1 mg of QD-MNSs in acetonitrile was mixed with 100 μg of carboxyl-terminated PLGA and 100 μg of PTX by sonication. The mixed organic suspension was emulsified in 500 mL of Milli-Q purified water and then sonicated using an energy output of 5 W. The organic solvent was removed from the oil-in-water emulsion under reduced pressure. The suspension was applied by applied external magnetic field, and carboxyl-functionalized PTX-PLGA-QD-MNSs were collected and washed three times with PBS. Amine reactive groups on the surface of the PTX-PLGA-QD-MNSs were obtained by amine coupling of ethylenediamine to carboxyl-functionalized PTX-PLGA-QD-MNSs. A carboxyl-functionalized PTX-PLGA-QD-MNS suspension was treated with ethylenediamine for 30 min at room temperature. Excess ethylenediamine was removed by external magnetic field, and amine-functionalized PTX-PLGA-QD-MNSs were collected and washed three times with PBS.

Conjugation of Anti-PSMA on the Surface of PTX-PLGA-QD-MNSs: Amine-functionalized PTX-PLGA-QD-MNSs (500 μg) were treated with 200 μL of 400 mM EDC and 200 μL of 200 mM NHS for 30 min at room temperature. The PTX-PLGA-QD-MNSs incorporated with amine-reactive NHS-esters were collected by applying magnetic field and washed with Milli-Q purified water three times to remove unreacted chemicals. An anti-PSMA solution was added with the NHS-activated PTX-PLGA-QD-MNSs for 2 h at room temperature and then washed three times with Milli-Q purified water.

***In Vitro* Cytotoxicity Assay:** Human PC3mm2 prostate carcinoma cells were cultured in Eagle's minimal essential medium (EMEM) supplemented with 5% (v/v) fetal bovine serum (FBS), nonessential amino acids, sodium pyruvate, vitamin A, and glutamine at 37 °C in a humidified atmosphere of 5% CO_2. Cells in exponential growth phase were harvested using 0.25% (w/v) trypsin/0.02% EDTA (w/v) solution. For cell viability experiments, PC3mm2 cells were plated at a density of 1000 cells/well in 96-well plates. Untreated PC3 cells plating at 1000 cells/well will reach confluence 4 days later and give OD values of MTT staining in linear range. After an overnight attachment period, cells were exposed for 96 h at 37 °C to various MNS populations at doses between 0.016 and 50 μg/mL. MNS suspensions were prepared in EMEM/5% FBS and dosed at 100 μL/well. During the final 2 h of incubation, 20 μL of 3-(4,5-dimethylthiazol-2-yl)-2,5-diphenyltetrazolium bromide (2 mg/mL in PBS) was added to each well. At the end of the incubation period, the medium was carefully aspirated, and the blue formazan complex dissolved in 100 μL of dimethyl sulfoxide. Absorbance of each well was quan-

tified at λ = 570 nm using a FluoStar Optima microplate reader (BMG Labtechnologies, Durham, NC). Cell viability was normalized to EMEM/5% FBS-treated vehicle control cells and expressed as %.

***In Vitro* Targeting:** To determine anti-PSMA-PTX-PLGA-QD-MNS binding to LNCaP cells, immunocytochemical studies were carried out. LNCap and PC3mm2 cells were fixed by incubating them in 4% (v/v) paraformaldehyde in PBS for 20 min at room temperature, blocked with 0.1% bovine serum albumin (5 min at room temperature), and then treated with anti-PSMA-conjugated PTX-PLGA-QD-MNSs and nontargeted PTX-PLGA-QD-MNS. After 30 min, the cells were washed with PBS three times and examined under the microscope (excitation = 560/40 nm, emission = 620/40 nm).

***Ex Vivo* Targeting:** *Ex vivo* fluorescence images of the mouse were taken with 720 nm excitation filter and 790 nm emission filter set using a Kodak 4000MM Whole-Mouse Image Station. Nu/nu nude mice, obtained from the National Cancer Institute, were 6−8 weeks old and typically weighed 18 g. Mice were anesthetized for imaging by beutal saline intraperitoneally, and the 250 μg dosage of anti-PSMA-PTX-PLGA-QD-MNSs dispersed in 100 μL of PBS was administrated *via* tail vein injection. After 30 min postadministration, the mouse was sacrificed. The excised organs from the control mouse and the treated mouse were placed in a same place, and the fluorescent image of the organs was taken. This study was approved by Institutional Animal Use and Care Committee (IACUC) at the University of Cincinnati, OH.

Acknowledgment. This research was supported in part by grants from the National Science Foundation (DGE-0333377) and the University of Cincinnati, Institute of Nanoscale Science and Technology.

REFERENCES AND NOTES

1. Wood, K. C.; Azarin, S. M.; Arap, W.; Pasqualini, R.; Langer, R.; Hammond, P. T. Tumor-Targeted Gene Delivery Using Molecularly Engineered Hybrid Polymers Functionalized with a Tumor-Homing Peptide. *Bioconjugate Chem.* **2008**, *19*, 403–405.
2. Inoue, Y.; Izawa, K.; Yoshikawa, K.; Yamada, H.; Tojo, A.; Ohtomo, K. *In Vivo* Fluorescence Imaging of the Reticuloendothelial System Using Quantum Dots in Combination with Bioluminescent Tumour Monitoring. *Eur. J. Nucl. Med. Mol. Imaging* **2007**, *34*, 2048–2056.
3. Qian, X.; Peng, X.-H.; Ansari, D. O.; Yin-Goen, Q.; Chen, G. Z.; Shin, D. M.; Yang, L.; Young, A. N.; Wang, M. D.; Nie, S. *In Vivo* Tumor Targeting and Spectroscopic Detection with Surface-Enhanced Raman Nanoparticle Tags. *Nat. Biotechnol.* **2008**, *26*, 83–90.
4. Moghimi, S. M.; Hunter, A. C.; Murray, J. C. Long-Circulating and Target-Specific Nanoparticles: Theory to Practice. *Pharmacol. Rev.* **2001**, *53*, 283–318.
5. Shekunov, B. Y.; Chattopadhyay, P.; Tong, H. H. Y.; Chow, A. H. L. Particle Size Analysis in Pharmaceutics: Principles, Methods and Applications. *Pharm. Res.* **2007**, *24*, 203–227.
6. Weissleder, R. A Clearer Vision for *In Vivo* Imaging. *Nat. Biotechnol.* **2001**, *19*, 316–317.
7. Jordan, A.; Scholz, R.; Wust, P.; Fähling, H.; Roland, F. Magnetic Fluid Hyperthermia (MFH): Cancer Treatment with Ac Magnetic Field Induced Excitation of Biocompatible Superparamagnetic Nanoparticles. *J. Magn. Magn. Mater.* **1999**, *201*, 413–419.
8. Hergt, R.; Dutz, S.; Müller, R.; Zeisberger, M. Magnetic Particle Hyperthermia: Nanoparticle Magnetism and Materials Development for Cancer Therapy. *J. Phys.: Condens. Matter* **2006**, *18*, S2919.
9. Neuberger, T.; Schöpf, B.; Hofmann, H.; Hofmann, M.; von Rechenberg, B. Superparamagnetic Nanoparticles for Biomedical Applications: Possibilities and Limitations of a New Drug Delivery System. *J. Magn. Magn. Mater.* **2005**, *293*, 483–496.
10. Shi, D.; Cho, H. S.; Chen, Y.; Xu, H.; Gu, H.; Lian, J.; Wang, W.; Liu, G.; Huth, C.; Wang, L.; *et al.* Fluorescent Polystyrene-Fe_3O_4 Composite Nanospheres for *In Vivo* Imaging and Hyperthermia. *Adv. Mater.* **2009**, *21*, 2170–2173.
11. Xu, H.; Cui, L.; Tong, N.; Gu, H. Development of High Magnetization Fe_3O_4/Polystyrene/Silica Nanospheres *via* Combined Miniemulsion/Emulsion Polymerization. *J. Am. Chem. Soc.* **2006**, *128*, 15582–15583.
12. Franchini, M. C.; Baldi, G.; Bonacchi, D.; Gentili, D.; Giudetti, G.; Lasciafari, A.; Corti, M.; Marmorato, P.; Ponti, J.; Micotti, E.; *et al.* Bovine Serum Albumin-Based Magnetic Nanocarrier for MRI Diagnosis and Hyperthermic Therapy: A Potential Theranostic Approach against Cancer. *Small* **2010**, *6*, 366–370.
13. Pan, D.; Caruthers, S. D.; Hu, G.; Senpan, A.; Scott, M. J.; Gaffney, P. J.; Wickline, S. A.; Lanza, G. M. Ligand-Directed Nanobialys as Theranostic Agent for Drug Delivery and Manganese-Based Magnetic Resonance Imaging of Vascular Targets. *J. Am. Chem. Soc.* **2008**, *130*, 9186–9187.
14. Liang, H.-F.; Chen, C.-T.; Chen, S.-C.; Kulkarni, A. R.; Chiu, Y.-L.; Chen, M.-C.; Sung, H.-W. Paclitaxel-Loaded Poly(L-Glutamic Acid)-Poly(Lactide) Nanoparticles as a Targeted Drug Delivery System for the Treatment of Liver Cancer. *Biomaterials* **2006**, *27*, 2051–2059.
15. Lu, Z.; Yeh, T.-K.; Tsai, M.; Au, J. L. S.; Wientjes, M. G. Paclitaxel-Loaded Gelatin Nanoparticles for Intravesical Bladder Cancer Therapy. *Clin. Cancer Res.* **2004**, *10*, 7677–7684.
16. Sahoo, S. K.; Ma, W.; Labhasetwar, V. Efficacy of Transferrin-Conjugated Paclitaxel-Loaded Nanoparticles in a Murine Model of Prostate Cancer. *Int. J. Cancer* **2004**, *112*, 335–340.
17. Koziara, J. M.; Lockman, P. R.; Allen, D. D.; Mumper, R. J. Paclitaxel Nanoparticles for the Potential Treatment of Brain Tumors. *J. Controlled Release* **2004**, *99*, 259–269.
18. Dunne, M.; Corrigan, O. I.; Ramtoola, Z. Influence of Particle Size and Dissolution Conditions on the Degradation Properties of Polylactide-*co*-Glycolide Particles. *Biomaterials* **2000**, *21*, 1659–1668.
19. Grayson, A. C. R.; Cima, M. J.; Langer, R. Size and Temperature Effects on Poly(lactic-*co*-glycolic acid) Degradation and Microreservoir Device Performance. *Biomaterials* **2005**, *26*, 2137–2145.
20. Reed, A. M.; Gilding, D. K. Biodegradable Polymers for Use in Surgery—Poly(glycolic)/Poly(lactic acid) Homo and Copolymers: 2. *In Vitro* Degradation. *Polymer* **1981**, *22*, 494–498.
21. Dong, Y.; Feng, S.-S. Poly(D,L-lactide-*co*-glycolide)/Montmorillonite Nanoparticles for Oral Delivery of Anticancer Drugs. *Biomaterials* **2005**, *26*, 6068–6076.
22. Ong, B. Y. S.; Ranganath, S. H.; Lee, L. Y.; Lu, F.; Lee, H.-S.; Sahinidis, N. V.; Wang, C.-H. Paclitaxel Delivery from PLGA Foams for Controlled Release in Post-Surgical Chemotherapy against Glioblastoma Multiforme. *Biomaterials* **2009**, *30*, 3189–3196.
23. Fonseca, C.; Simões, S.; Gaspar, R. Paclitaxel-Loaded PLGA Nanoparticles: Preparation, Physicochemical Characterization and *In Vitro* Anti-tumoral Activity. *J. Controlled Release* **2002**, *83*, 273–286.
24. Jin, C.; Bai, L.; Wu, H.; Song, W.; Guo, G.; Dou, K. Cytotoxicity of Paclitaxel Incorporated in PLGA Nanoparticles on Hypoxic Human Tumor Cells. *Pharm. Res.* **2009**, *26*, 1776–1784.
25. Guo, Y.; Shi, D.; Cho, H.; Dong, Z.; Kulkami, A.; Pauletti, G. M.; Wang, W.; Lian, J.; Liu, W.; Ren, L.; *et al. In Vivo* Imaging and Drug Storage by Quantum-Dot-Conjugated Carbon Nanotubes. *Adv. Funct. Mater.* **2008**, *18*, 2489–2497.
26. Mu, L.; Seow, P. H. Application of TPGS in Polymeric Nanoparticulate Drug Delivery System. *Colloids Surf., B* **2006**, *47*, 90–97.
27. Desai, N.; Trieu, V.; Yao, Z.; Louie, L.; Ci, S.; Yang, A.; Tao, C.; De, T.; Beals, B.; Dykes, D.; *et al.* Increased Antitumor Activity, Intratumor Paclitaxel Concentrations, and Endothelial Cell Transport of Cremophor-Free, Albumin-Bound Paclitaxel, Abi-007, Compared with Cremophor-Based Paclitaxel. *Clin. Cancer Res.* **2006**, *12*, 1317–1324.